Development of Simple and High-Performance Technology for Turbine

TANIMITSU Haruyuki : Advanced Technology Department, Research & Engineering Division, Aero-Engine & Space Operations
NAKAMATA Chiyuki : Doctor of Engineering, Advanced Technology Department, Research & Engineering Division, Aero-Engine & Space Operations
FUJIMOTO Syu : Engine Technology Department, Research & Engineering Division, Aero-Engine & Space Operations
AOKI Yasuhiro : Doctor of Engineering, Materials Technology Department, Research & Engineering Division, Aero-Engine & Space Operations
ISHIZAKI Masato : Manager, Production Technology Development Department, Production Engineering Center, Corporate Research & Development

To reduce direct operating costs of environmentally compatible engine for small aircraft, higher loading turbine without performance decrement was studied. The study was carried out for shock wave control and feasibility of counter-rotation turbine system. The aerodynamic performance was verified by the rig tests. Another outstanding advancement was novel cooling technologies. There were two key technical features: multi-slot internal cooling system and newly-developed film cooling hole to improve film effectiveness. These new cooling systems were validated in the cascade rig tests. To evaluate the applicability of Japanese single crystal superalloys to low cost HPT blades, studies of ingot, casting and heat treatment processes of the superalloys were conducted for the HPT blades. The laser-CVD process was studied as the coating method of the top layer of TBC. Trial coating on turbine blades was carried out, and the technical problems of the method for application were explained.

1. Introduction

In developing the environmentally compatible engine for small aircraft (ECO engine), our primary goal is to achieve a substantial reduction in direct operating costs, including acquisition, maintenance and fuel costs. For a turbine comprised of multistage rotor blade and stator vane cascades and other parts made mostly of expensive nickel-based materials with large specific gravities, simple high-performance design techniques are required to reduce the number of stages and thereby the weight and cost while maintaining a high efficiency. To materialize a high-loaded high-pressure single-stage turbine with high performance, we developed the shock wave control and the counter rotation technologies that should enable us to reduce interactions between high- and low-pressure turbines. As cooling technologies to realize a simple and efficient turbine, we studied the multi-slot cooling configuration [(1)] and high-efficiency film holes[(2)]. The configurations were optimized by using heat transfer CFD (Computational Fluid Dynamics) and other analysis techniques. The design results were evaluated and the design techniques used were validated by cooling performance tests. Some analyses and tests were conducted through collaboration with JAXA (Japan Aerospace Exploration Agency) and Tokyo University of Agriculture and Technology. TMS-138, an advanced next-generation single crystal superalloy with high-temperature strength characteristics superior to those of commonly used single crystal superalloys for turbine airfoils, was jointly developed by NIMS (National Institute for Materials Science) and IHI. TMS-138 was used as a test specimen, and research and development activities were conducted to reduce costs and improve the manufacturability of TMS-138 while taking care to maintain its characteristics. To optimize production conditions, we developed a YSZ (Yttria Stabilized Zirconia) coating formation technology using a laser CVD (Chemical Vapor Deposition) method, and clarified the technical problems related to forming a TBC (Thermal Barrier Coating) on a turbine blade member.

This paper describes the results of activities conducted in the ECO engine project to develop advanced technologies concerning aerodynamics, cooling, materials and production of a new turbine engine.

2. Turbine aerodynamic design techniques

2.1 Technology for controlling shock waves on rotor blades of a high-pressure turbine

Since Mach number increases in a high-loaded high-pressure turbine, shock wave occurs, causing aerodynamic performance to deteriorate, interference with a low-pressure turbine, and interaction loss to increase. Controlling shock wave is the key to reduce interaction loss.

To identify the airfoil shape that enables us to reduce the shock wave loss of rotor blades, four airfoil shapes were experimentally designed through CFD analyses by changing the intensity of a shock wave occurring between blades. **Figure 1** shows the Mach number distributions on the airfoil surface of each airfoil shape. It is apparent from this figure that deceleration at the suction side downstream of peak Mach number depends on airfoil shape. Based on these four airfoil shapes, five different airfoils were designed and manufactured. The surfaces of each airfoil have cooling holes to simulate actual turbine configurations. Airfoil Type I and II are baseline airfoils, Type III and IV are shock wave controlled airfoils "A" and "B", and Type V is an airfoil having a larger trailing edge thickness. **Table 1** lists these five airfoil types.

Table 1 Five airfoil types

	Airfoil shape	Cooling hole position
Type I	Baseline airfoil	Cooling holes on the suction side surface are located closer to the leading edge. Cooling holes around the trailing edge are located on the pressure-side surface of an airfoil near the trailing edge.
Type II	Baseline airfoil	The backmost row of cooling holes on the suction side surface is located further back than that of Type I. Cooling holes around the trailing edge surface are located in the same position as those of Type I.
Type III	Shock wave controlled airfoil A	Same as the Type I
Type IV	Shock wave controlled airfoil B	Same as the Type I
Type V	Airfoil having a larger trailing edge thickness	Cooling holes on the suction side surface are located in the same position as Type I. Cooling holes around the trailing edge surface are located in the middle of the trailing edge.

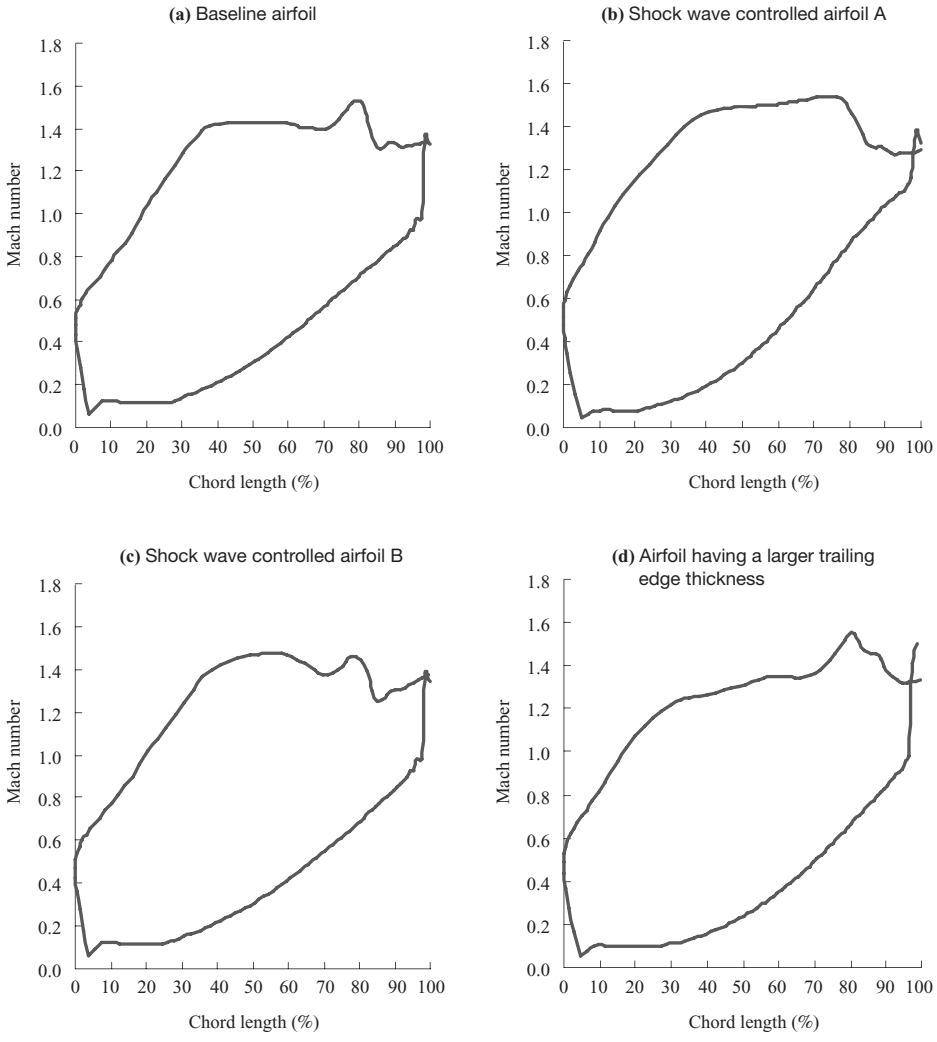

Fig. 1 Mach number distribution on airfoil surface

The performance of each airfoil was measured by a high-speed wind tunnel test for two-dimensional cascades that enable to conduct measurement in high Mach number region. **Figure 2** shows the appearance of a cascade for the high-speed wind tunnel test. **Figure 3** shows the total pressures measured by traversed probe at a mid-span and cascade exit position; the total pressures are expressed as normalized loss coefficients relative to exit Mach numbers. **Figure 4** shows the total pressures that are expressed as shock wave strengths. **Figure 5** shows loss coefficient distributions relative to exit Mach numbers in a case of changing the cooling hole positions on the suction-side surface of the baseline airfoil shape.

It is apparent from **Figs. 3** and **4** that although the airfoil aerodynamic performance of Type I is stable in subsonic and transonic speed regions, both loss and shock wave strength increase in high Mach number regions. Although the loss of Type III is small in a high Mach number region, it increases sharply in subsonic and transonic speed regions. In addition, in a region of high Mach numbers of 1.3 or larger, the shock wave strength of Type III is larger than that of Type IV. Type IV has the most stable performance; there is no significant loss in the range of exit Mach numbers from 1.0 to 1.4 which corresponds to the assumed engine operating range, and no sharp increase in the shock wave strength is observed. Although Type V was expected to be able to weaken wake by blowing cooling air from the center of a trailing edge, both loss and shock wave strength increase rapidly since the thickness of the trailing edge in a high Mach number region is larger than that of other types. **Figure 5** indicates that loss is smaller at exit Mach numbers of 1.2 or larger with Type I compared with Type II, whose position of cooling holes on the suction-side surface is near the leading edge.

As is clear from the above, Type IV has a stable airfoil aerodynamic performance since the shock wave strength is restrained over the entire engine operating range, compared with other types. This indicates that the airfoil shape of Type IV is ideal for the rotor blade

Fig. 2 Tested airfoil

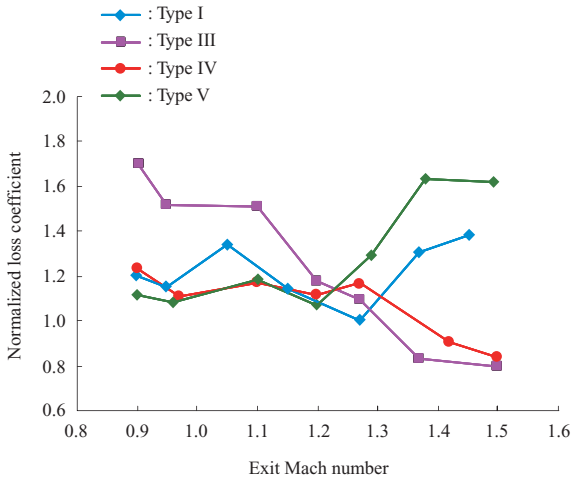

Fig. 3 Normalized loss coefficient by airfoil types

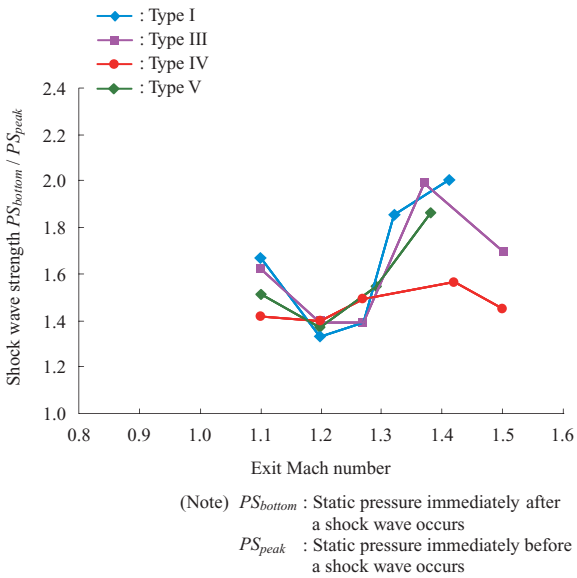

Fig. 4 Shock strength by airfoil types

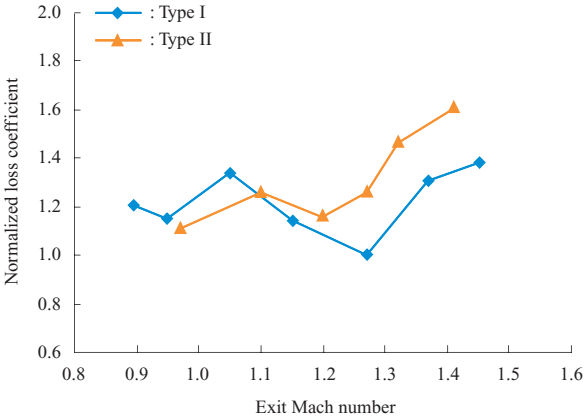

Fig. 5 Changes in loss coefficient by different cooling hole position on airfoil suction side

of a high-loaded high-pressure turbine. It was also found that for a high-loaded high-pressure turbine airfoil, the positions of the cooling hole on the suction side surface affect the loss, specifically, the airfoil aerodynamic performance is worse if cooling air is blown out in high Mach number regions.

2. 2 Counter rotation technology

If the pressure ratio achieved by conventionally designed two stages turbine is tried to be achieved by high-loaded high-pressure single-stage turbine, swirl (tangential velocity component) usually remains at the high-pressure turbine exit.

Rotating high- and low-pressure turbines in opposite directions is called "counter rotation." Counter rotation is a promising technology that swirl at the exit of a high-pressure turbine can be utilized effectively to reduce the loss caused by interactions between high- and low-pressure turbines.

To validate this technology, airfoil designs for stator vane and rotor blade of high-pressure turbine with first-stage stator vane of low-pressure turbine were conducted. Unsteady CFD analyses for the 1.5 stages were performed for counter-rotating high- and low-pressure turbines. As a result, it was verified that interactions could be reduced.[3]

High-pressure turbine and first-stage stator vane of low-pressure turbine were designed and manufactured, and their performance was evaluated by conducting 1.5-stage turbine rotating tests. For the first-stage stator vane of a low-pressure turbine, two rotation configurations were used to measure the effect of counter rotation: the counter rotation configuration and the conventionally used co-rotation configuration. **Figure 6** shows the cross-sectional shapes of these stator vanes and rotor blade at a mid-span. It should be noted that the turning angle of the first-stage stator vane of a low-pressure turbine tested in the counter rotation configuration is smaller than that of the first-stage stator vane tested in the co-rotation configuration. **Figure 7** shows the cross section of a 1.5-stage turbine rotating testing rig model, and **Fig. 8** shows mounted HPT module on the testing rig. In this test, a blow-out of cooling air needed to operate a high-pressure turbine was simulated to evaluate turbine performance. In the 1.5-stage rotating test, performance mapping of a high-pressure turbine was conducted, and aerodynamic measurement was conducted at the exit of a high-pressure turbine and at the exit of the first-stage stator vane of a low-pressure turbine to evaluate interaction. **Figure 9** shows the performance mapping of a high-pressure turbine. The efficiency obtained by measurements is higher by about 0.8 points than the design target, indicating that the technology for designing a high-performance high-loaded single-stage turbine has been demonstrated.

Figure 10 compares distribution of the loss coefficient for the first-stage stator vane of a low-pressure turbine in the counter rotation configuration and that in the co-rotation configuration. The loss of the stator vane in the counter rotation configuration is far smaller than that of the stator blade in the co-rotation configuration, except around the tip region.

Figure 11 compares the measurements conducted at the exit of the stator vane of a low-pressure turbine

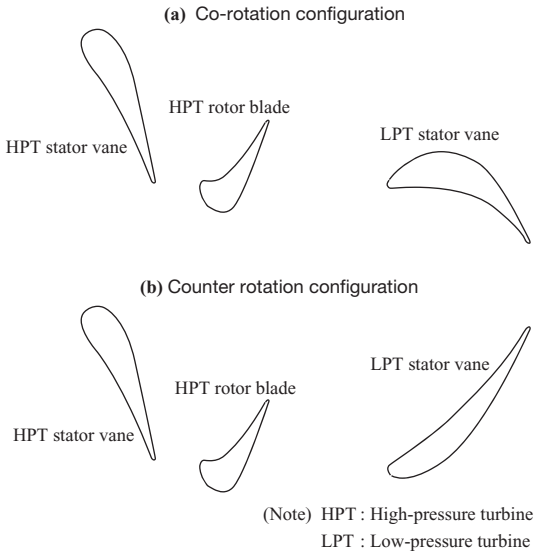

Fig. 6 Airfoil cross sections of HPT and LPT first nozzle

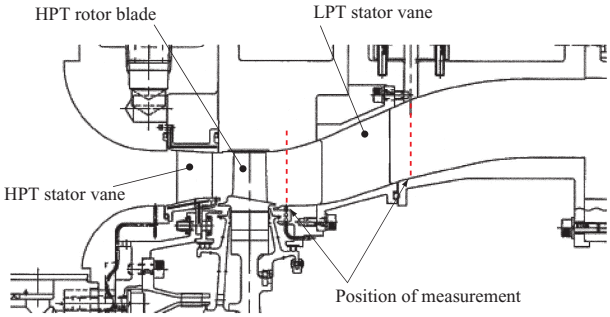

Fig. 7 Cross section of turbine rig

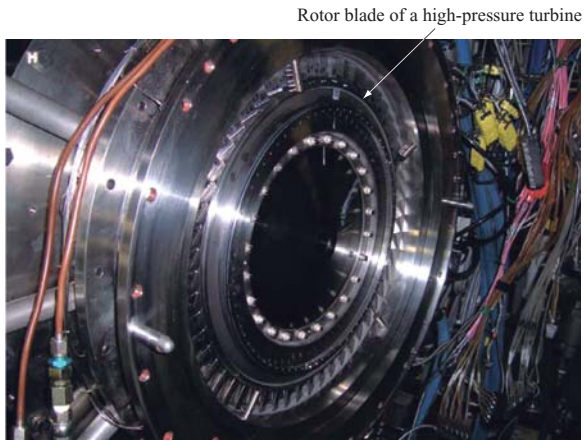

Fig. 8 Installed HPT Modules

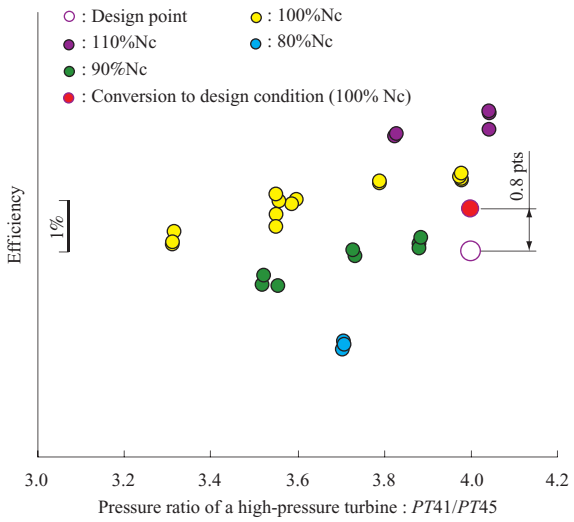

(Note) *PT*41 : Total pressure at the inlet of a high-pressure turbine
*PT*45 : Total pressure at the exit of a high-pressure turbine
Nc : Corrected rotating speed

Fig. 9 HPT Performance test results

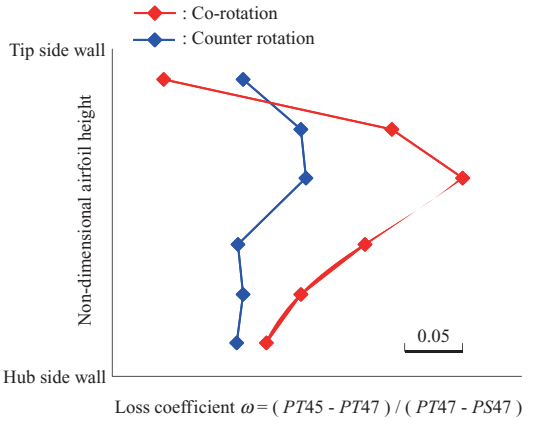

(Note) *PT*47 : Total pressure at the exit of LPT stator vane
*PS*47 : Static pressure at the exit of LPT stator vane

Fig. 10 Loss Coefficient of LPT stator vane

with the results of unsteady CFD analyses for the 1.5 stages. Because the results of CFD analyses were in good agreement with the test results, it was confirmed that CFD analyses performed in this study was verified. **Figure 12** compares the loss coefficient of the stator vane of a low-pressure turbine obtained through unsteady CFD analyses with that obtained through steady CFD analyses. Since the difference between the loss from unsteady CFD analyses and that from steady CFD analyses is considered to be caused by interference between cascades, it is apparent from **Fig. 12** that the loss caused by interactions between the high-pressure turbine flow and the first-stage stator vane of a low-pressure turbine can be reduced by adopting counter rotation.[4]

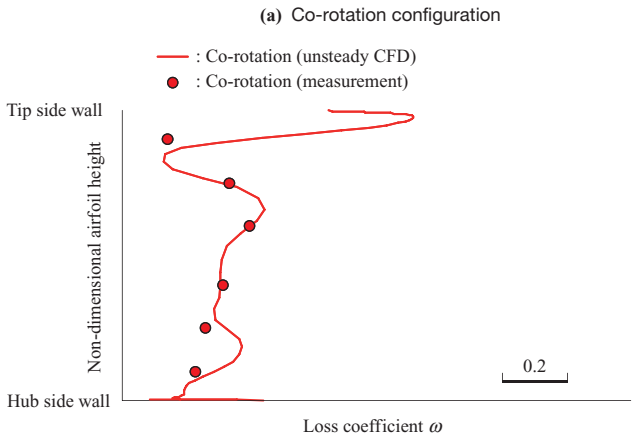

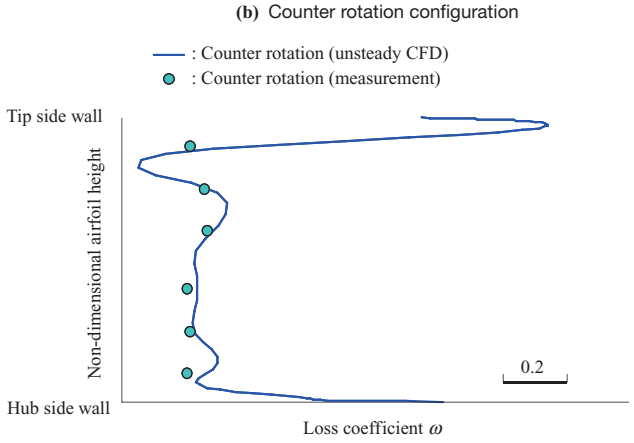

Fig. 11 Comparison between CFD and measurements

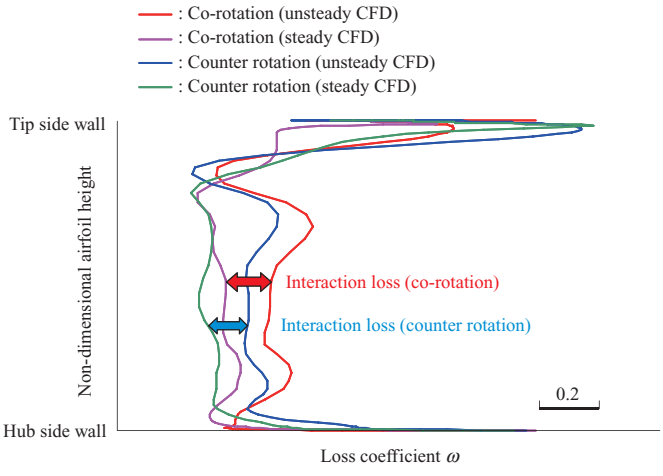

Fig. 12 Interaction loss at LPT stator vane

The results of the 1.5-stage rotating tests and CFD analyses described above demonstrate the performance of a high-loaded high-pressure single-stage turbine. That counter rotation can reduce interactions was verified based on the results of CFD analyses which had been validated based on test data, indicating that we successfully had demonstrated the counter rotation

technology necessary to design a high-loaded high-pressure single-stage turbine.

3. Turbine cooling design technology

3. 1 Multi-slot cooling configuration

The internal structure of a turbine airfoil for a small engine should be simple and a complicated cooling system should be avoided as much as possible. For example, a double wall structure that is manufactured by embedding inserts inside an airfoil, a conventional cooling configuration often applied to turbine stator vanes, makes the production complicated and difficult, particularly if the size of an airfoil is small. As part of this study, a multi-slot cooling configuration suited to cooling the turbine stator vane of a small engine was developed to simplify the cooling system. As shown in **Fig. 13**, this multi-slot cooling configuration has multiple slots formed by ribs set in a stagger inside an airfoil. After cooling air enters the inside of an airfoil from the inlet, it passes through each slot and generates high-heat transfer coefficient especially at a turning point of flow, thus making it possible to effectively cool the internal surface of an airfoil. In addition, because the multi-slot cooling configuration does not require such parts as inserts, the multi-slot cooling configuration can be used for an airfoil designed in a highly three-dimensional shape that curves in the span direction.

As the results of basic cooling performance tests conducted in early development stages, it was confirmed that the multi-slot cooling configuration could achieve high enough cooling effectiveness under the test condition.[1] To verify the cooling performance of this multi-slot cooling configuration under conditions closer to actual operating conditions, tests were conducted on a cooling nozzle made on the same scale as that of an actual engine by using the sector cascade test rig shown in **Fig. 14** that simulates the actual operating environment. In **Fig. 14**, a stator vane designed with a multi-slot cooling configuration is seen at the center of a cascade. **Figure 15** shows the appearance of this cooled vane tested. Goals of this study include not only

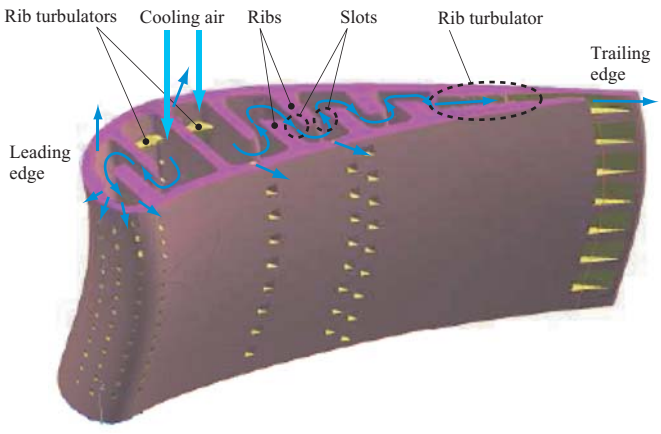

Fig. 13 Schematic of multi-slot internal cooling

Fig. 14 Annular sector cascade rig

the verification of cooling performance of the multi-slot cooling configuration but also the verification of whether a turbine designed with the multi-slot cooling configuration can be manufactured using existing precision casting and processing techniques. By making a prototype of a cast airfoil to supply for the cascade tests, it was confirmed that the multi-slot cooling configuration suited to a three-dimensional airfoil shown in **Fig. 15** can be manufactured using the existing manufacturing techniques at costs equivalent to the costs of conventional cooling configurations.

Figure 16 shows the airfoil surface temperature distribution and the cooling effectiveness at a mean section which were obtained from the cascade tests. The airfoil surface temperature distribution shown in this figure was measured using an infrared radiation imaging system, and measured absolute values

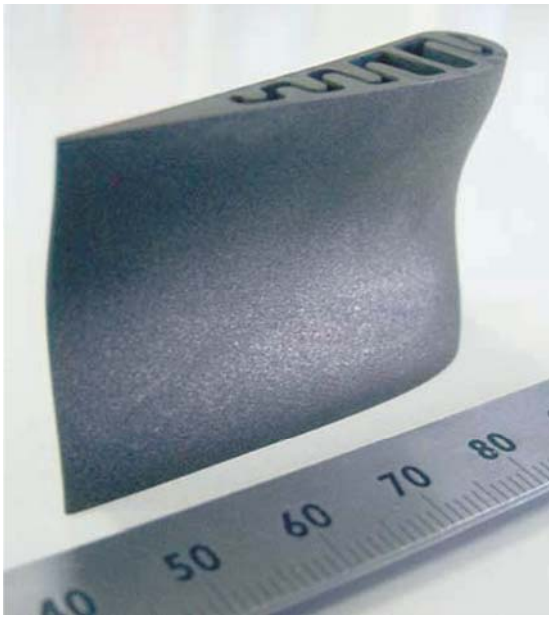

Fig. 15 Photograph of multi-slot cooled vane

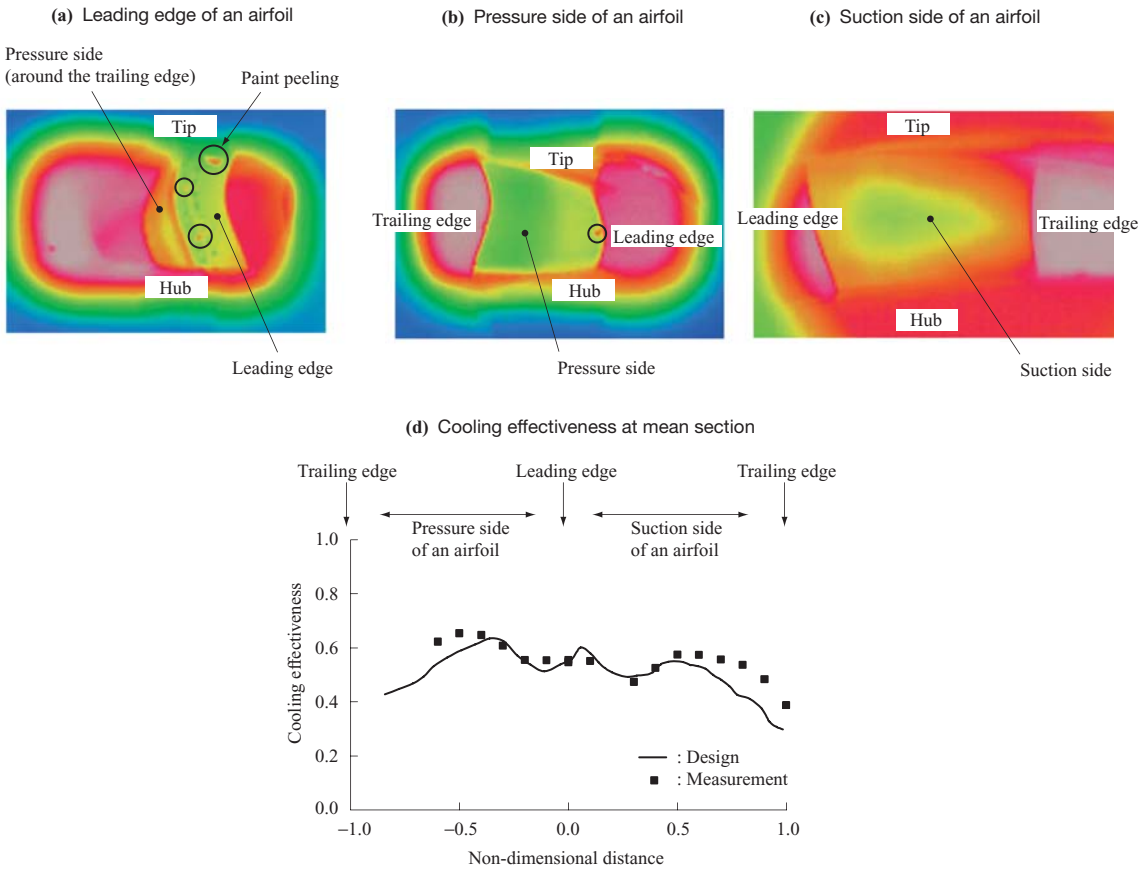

Fig. 16 Measured surface temperatures on vane surfaces

were calibrated using a temperature measured by a thermocouple installed on the airfoil surface. The distribution indicates that the surface temperatures are almost uniform. Although local hot spots are not observed, it should be noted that the temperature around the endwall at the trailing edge of the airfoil is somewhat higher than at other parts. This is more noticeable on the suction side than on the pressure side. A possible cause is the effect of secondary flow occurring between vanes. According to the theory of secondary flow, vortices caused by secondary flow gradually become larger around the endwalls between vanes, and become largest around the suction side of the airfoil surface of a trailing edge. It was considered that the heat transfer coefficient of main flow at the trailing edge part on the suction side would increase from the effect of these vortices and temperature would subsequently increase. There is the possibility that the parts where hot spots are observed may not have been cooled enough since due consideration was not given to the effect of the secondary flow of the main flow at the cooling design stage. On the other hand, a graph comparing designed and measured cooling effectiveness values at mean section evidently shows that the cooling effectiveness verified in tests is almost equal to the designed value.

It was verified based on the results described above that the multi-slot cooling configuration developed as part of the ECO engine project can be used for a small-size turbine airfoil to which it is difficult to apply a complicated cooling system and also for a three-dimensional airfoil at reasonable production costs equivalent to those of conventional cooling systems.

3. 2 High-performance film cooling hole

Another technology developed in the ECO engine project concerns a new film cooling hole geometry that allows us to achieve higher film-cooling effectiveness.

This technology aims to reduce the amount of cooling air by increasing the film effectiveness and thereby reducing the fuel consumption of an engine. In the development, CFD analysis was used for a systematic study to know how to modify film hole shape to improve film cooling effectiveness. And CFD analysis was also used to seek the optimum shape. It is important to improve the film effectiveness while minimizing disadvantages such as increasing the heat transfer coefficient of the main flow, inducing loss through mixing with the main flow, making the shape complicated, or increasing the production cost. **Figure 17** compares the new hole acquired through optimization with the conventional hole. The new hole has a unique arrowhead form at the hole exit because the shape is expanded sideways to prompt film cooling flow to be directed laterally (within a limitation that the effective area expansion rate is equivalent to that of conventional

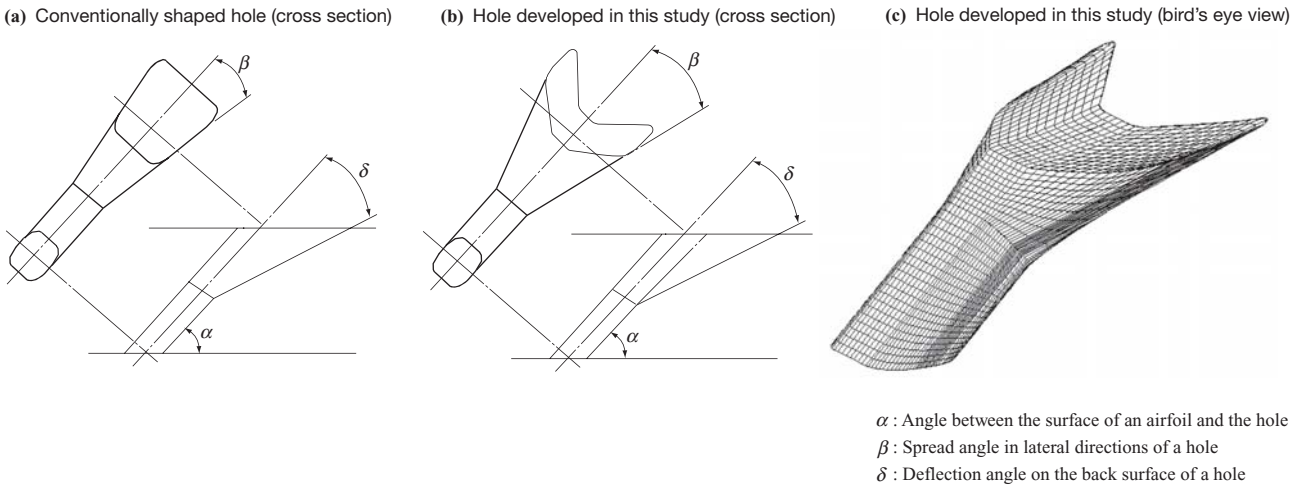

Fig. 17 Comparison of film cooling hole geometries

cooling holes). If film flow can be smoothly directed laterally as intended, a more uniform film layer can be formed on the airfoil surface and, as a result, the average film effectiveness can be improved.

A film hole can be machined to this shape by using the existing electrical discharge machining method conventionally used to make conventional shaped film holes; special machining techniques are not required.

A cooling performance test was then conducted on the airfoil with this new optimally designed high-performance film hole. **Figure 18** shows the experimental apparatus and the film cooled vane used in the test. As shown in **Fig. 18**, pressure-sensitive paint was applied to the part downstream of the film hole on the suction- and pressure-side surfaces of the airfoil to measure the film effectiveness. In the test, light was cast from outside the test equipment through a window on the part on the airfoil where paint was applied. Since the pressure sensitive paint emits light according to the light intensity proportional to oxygen partial pressure in atmospheric air, the way the pressure sensitive paint emits light according to the oxygen concentration on the airfoil surface can be photographed using a camera. If a gas other than air (nitrogen gas was used in this test) is used as a working fluid to be blown out of the film hole on the cooling side, it is possible to acquire precise film effectiveness data from data on the luminescence intensity extracted from photographed images. **Figure 19** compares the film effectiveness on both the suction and pressure sides of the newly developed hole with that of the conventional shaped hole. It is apparent from **Fig. 19** that the film effectiveness of the newly developed film hole is higher on both suction and pressure sides than that of the conventional shaped hole. Particularly, there is a marked increase in the film effectiveness on the suction side.

The mechanism of how the film efficiency can be improved was clarified based on the results of fluid analyses. In the case of the conventional film hole, a pair of mutually counter rotating vertical vortexes occurs where main flow interferes with film air flow, as shown in **Fig. 20**. These vortexes work on film flow so that the film flow is forced to deflect its course off the wall surface while, at the same time, the main flow of

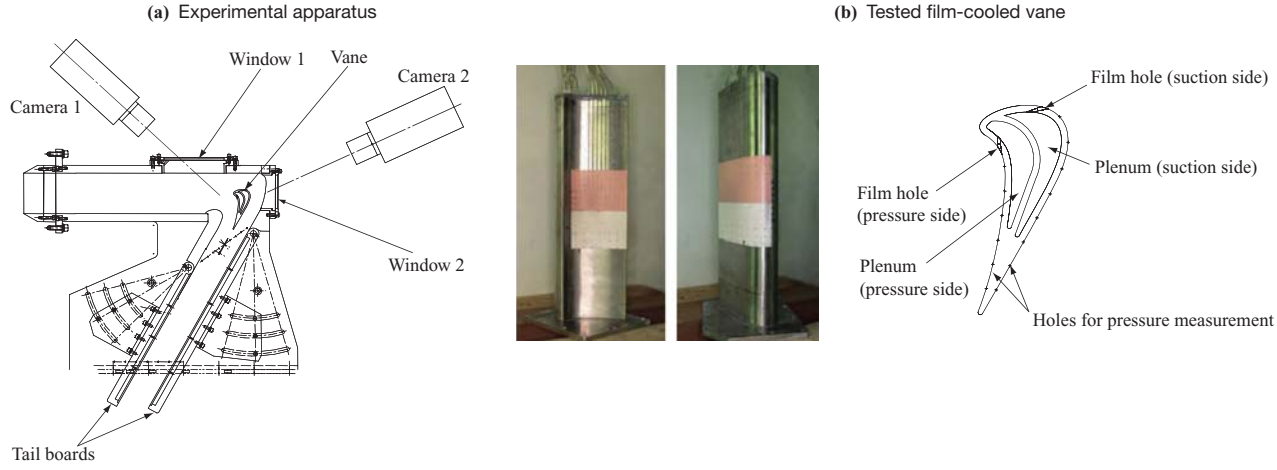

Fig. 18 Experimental apparatus and tested film-cooled vane

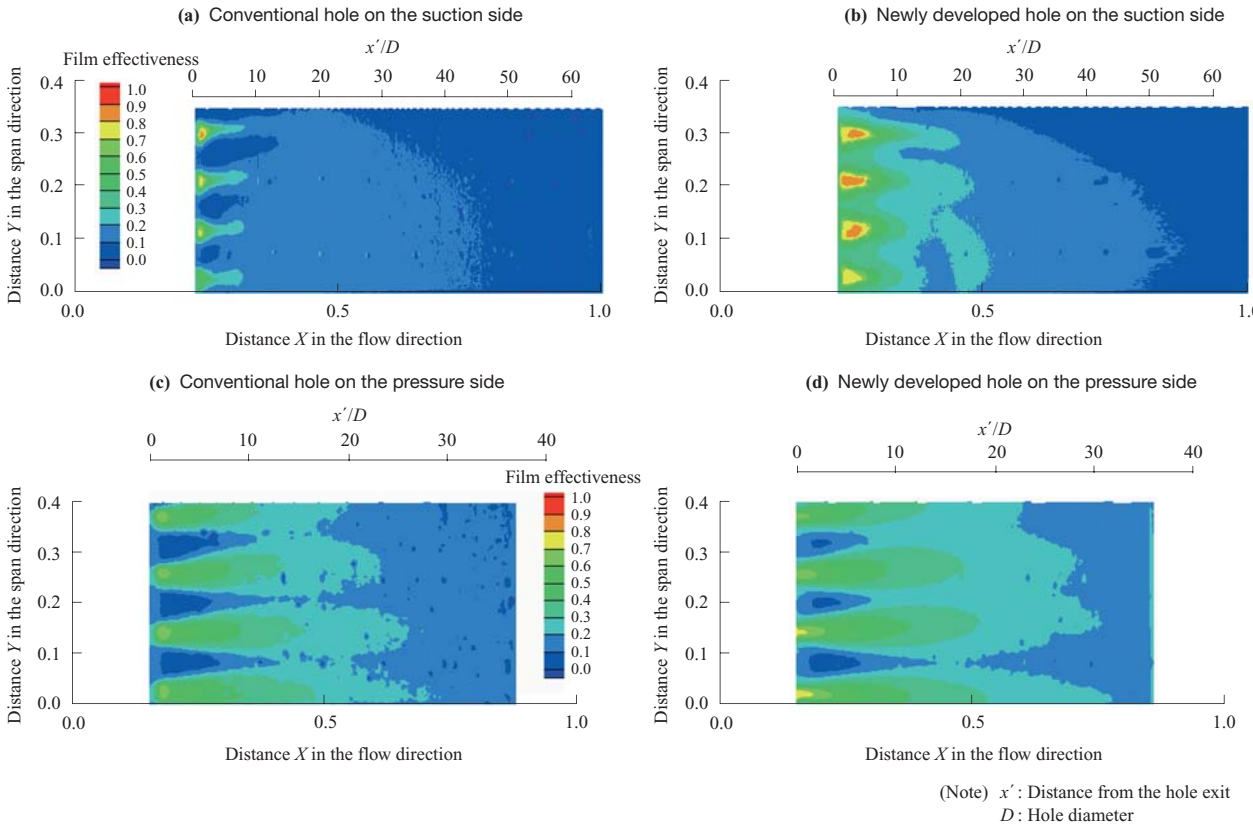

Fig. 19 Comparison of measured film effectiveness

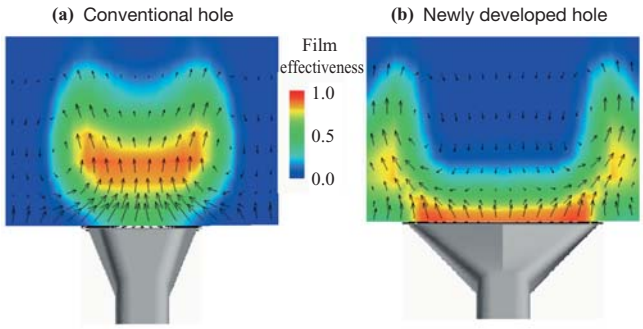

Fig. 20 Calculated secondary velocity vectors and film effectiveness near the hole exit

high-temperature gas is drawn from the side toward the wall surface. Although similar vertical vortexes occur with the newly developed film, special mention must be made of the fact that the vortexes observed with the newly developed film rotate in the reverse direction to that of the conventional hole. This counter rotation of the vortexes causes the film flow to be pushed against the wall surface, and the film flow continues traveling sideways along the wall surface. It is thought that the film effectiveness is higher with the newly developed film hole because of this counter rotation effect.

It was demonstrated from the results described above that if the high-performance film hole developed as part of the ECO engine project is used, a vortex structure changes on the airfoil surface and the degree of mixing with main flow is inhibited and, as a result, cooling performance can be substantially increased. It should also be noted that existing machining techniques can be used to make this new film hole.

4. Turbine materials technology

4. 1 Technology for production of blades made of advanced single crystal materials

The production processes of blade castings consist of ingot production, single crystal casting, heat treatment, and inspection. **Table 2** compares the chemical composition of advanced single crystal superalloy TMS-138 used in this research with the existing alloy CMSX-4, which already used for blades of civil engines. Because TMS-138 contains a larger amount of Re compared with CMSX-4 and also contains Ru in the platinum group, the material cost is higher. To reduce the cost of blade castings, the feasibility of applying the technology for production of low-cost castings was studied.

Table 2 Chemical compositions of CMSX-4 and TMS-138 (wt%)

Material tested	Chemical composition										
	Co	Cr	Mo	W	Al	Ti	Ta	Hf	Re	Ru	Ni
CMSX-4	9.6	6.4	0.6	6.4	5.6	1.0	6.5	0.1	3.0	-	60.8
TMS-138	5.9	2.9	2.9	5.9	5.9	-	5.9	0.1	4.9	2.0	63.6

(1) Technology for reusing scrapped materials (ingot production)
(2) Casting technology of two layers (casting)
(3) Technology of simplified age heat treatment (heat treatment)

4.1.1 Technology for reusing scrapped materials

Quantitative analysis of the chemical composition for scrapped material was performed in order to verify the appropriateness of reusing scrapped materials to contribute greatly to reducing the material cost. Scrapped materials to be reused were selected and the compounding ratio was determined based on the amount of trace elements mixed in the scrapped materials. Ingots and single crystal coatings were produced by mixing scrapped materials with virgin materials. The chemical composition of the alloy was checked through quantitative analysis, and it was verified that the segregation of the composition does not occur and there is no effect on high-temperature characteristics. Therefore, it was concluded that material costs can be reduced by reusing scrapped materials.

4.1.2 Casting technology of two layers

In the casting process, the casting cost per blade can be reduced by increasing the number of blades cast per mold. A method of casting multiple blades per mold by using the generally used single crystal casting method [5] and by mounting blades in a two-tier setup was proposed, as illustrated in **Fig. 21**. Before starting to cast airfoils, casting conditions were optimized using casting simulations. It was confirmed from the results of casting tests conducted that this low-cost casting method can be introduced although the appropriateness of this method was verified only at the level of prototyping.

4.1.3 Technology of simplified age heat treatment

To maximize the strength characteristics of existing single crystal superalloys (for example, CMSX-4), it is generally understood that solution heat treatment and primary and secondary aging heat treatments are required. To reduce costs and simplify these heat treatment processes, a test specimen was prepared by changing the time of secondary aging heat treatment, and the microstructure and strength of this test specimen were evaluated.

Figure 22 shows electron microscope images of test specimens subjected to secondary aging heat treatment of 0 hours (no heat treatment), 5, 10 and 20 hours. The γ' phase of test specimens subjected to these time lengths of heat treatment showed almost uniformly (well aligned cuboidal γ'), and there was no difference in the sizes of the γ' phase. It was verified from these results that the consistency of the γ' phase is very good irrespective of the time length of the heat treatment and that secondary aging heat treatment is unnecessary since the cooling γ' phase occurs between γ' phases. A test specimen was prepared by subjecting it to primary aging heat treatment only ; secondary aging heat treatment was not conducted, data on the creep rupture strength of this test specimen was taken, and the data was organized based on stress Larson-Miller parameter functions. **Figure 23** shows the data on the creep rupture strength organized this way. For the purpose of comparison, the results of a test performed on the conventionally used alloy CMSX-4 and those of a test performed on TMS-138 subjected to 20-hour aging heat treatment are also shown in **Fig. 23**.[6] Creep rupture test specimens without secondary aging heat treatment are not very different from those of test specimens with secondary aging heat treatment. It was clear that TMS-138 creep rupture strength of the test specimens prepared by changing the time length of secondary aging heat treatment is superior to that of CMSX-4 in that it exhibits excellent high-temperature strength over the entire stress range in which measurements were taken. It was thought, therefore, that there is a

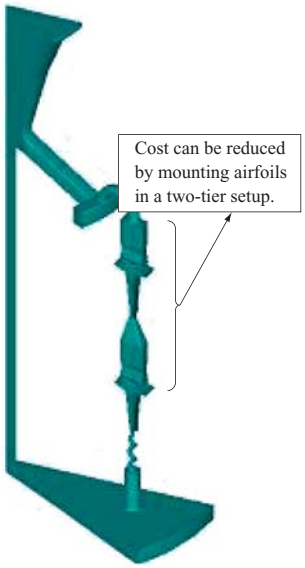

Fig. 21 Model of low cost casting process using casting simulation

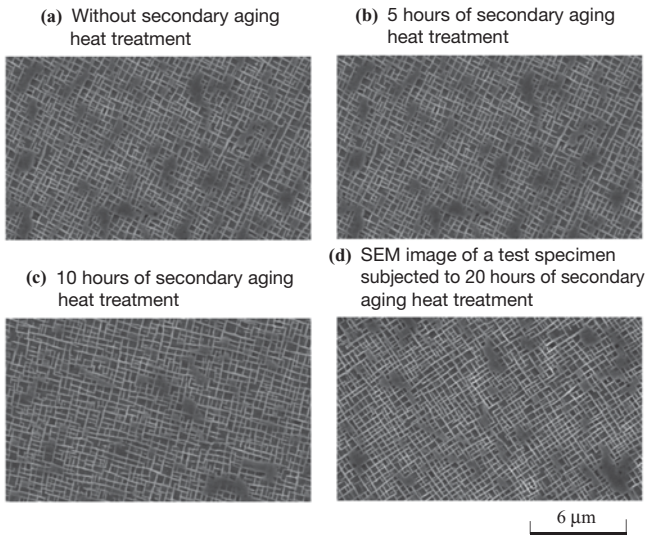

Fig. 22 SEM Images of secondary age heat treatments

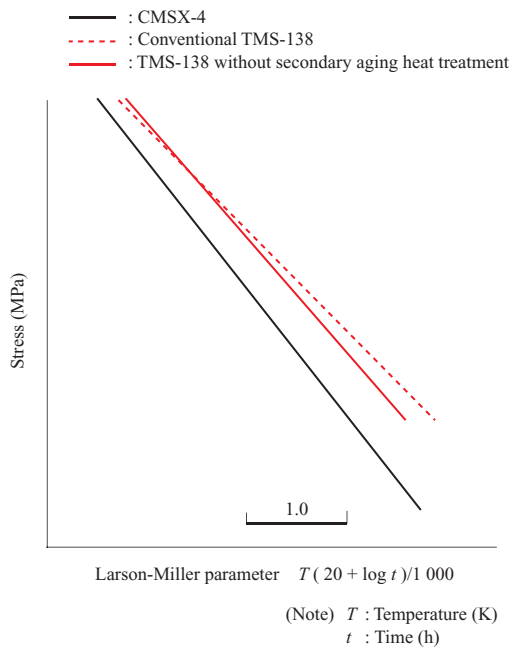

Fig. 23 Comparison of creep rupture strength

good prospect of simplifying the process by omitting the step of secondary aging heat treatment needed for conventionally used alloys.

Based on the results described above, the feasibility of applying the technology for reducing costs of ingot production, casting and heat treatment to the next-generation single crystal superalloys was considered to be very high. By applying this technology, it may be possible to manufacture single crystal turbine blades with superior characteristics without a substantial increase in costs, compared with the costs of manufacturing conventionally used single crystal superalloys (such as CMSX-4).

5. Turbine production technology (Technology for forming TBC by applying CVD)

EB-PVD (Electron Beam-Physical Vapor Deposition) is widely used in place of thermal spray coating as a technology for forming a top TBC (Thermal Barrier Coating) since EB-PVD makes it possible to form a microstructure suitable for TBC. CVD (Chemical Vapor Deposition) is a candidate alternative technology that allows a microstructure to be controlled and the process costs to be reduced at the same time to replace EB-PVD. To control the microstructure of a coating layer with the CVD method, sufficient energy must be supplied for the crystal growth. In this study, we developed a CVD coating method of TBC of yttria stabilized zirconia employing laser heating which enables it to supply a large energy to a limited, small area to grow crystals of ceramic coatings on a member made of metallic material with limited heat resistance.

The material used is dipivaloylmethanate (DPM) complexes containing zirconium and yttrium (supplied by Showa Denko KK). The DPM complexes are used as metallic element source gases for the CVD process. Because the DPM complexes start thermal decomposition at low temperatures around 300°C, extra care must be taken in controlling their temperatures. The CVD source gases used were two types of DPM materials carried with argon and mixed together, and oxygen introduced to a reaction chamber through a coaxial cylindrical nozzle.

YSZ coating formation tests were carried out using a test specimen of a button-shaped nickel-base alloy substrate with an aluminized layer on the outer surface, and the conditions for formation of a columnar-like crystal coating were investigated. The substrate was subjected to preliminary oxidation treatment in air in order to prevent the TBC layer on an aluminized surface of the nickel-based alloy from spalling. Coating formation parameters, including laser output, source gas flow rate, reaction pressure, and distance from the source gas nozzle to the substrate were examined, and the conditions to form facets which show desired growth of columnar-like crystals as a TBC layer were found (see **Fig. 24**).

Based on the coating formation conditions from the results of coating tests on button-shaped test specimens, TBC formation tests were carried out on a turbine blade, and it was confirmed that a coating can be formed on the entire surface of a turbine member having a complicated three-dimensional curved surface shape. During the coating test, a member was moved against the fixed source gas nozzle so that consecutive reactions took place and a coating was formed on the entire surface of the airfoil (see **Fig. 25**). The coating formed on the airfoil had parts where facets were apparent, and also parts where amorphous conditions were observed. Parts where amorphous conditions are observed are considered to be out of the center of laser radiation, where the amount of energy supplied was not enough for the crystal growth. To form a fully crystallized coating

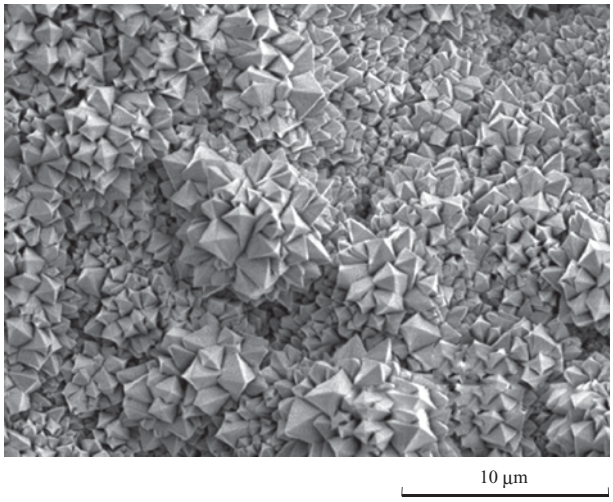

Fig. 24 Surface structure of YSZ coating obtained by laser-CVD

Fig. 25 A turbine blade with YSZ coating by laser-CVD

uniformly on the entire airfoil surface, it is necessary to establish technology to supply sufficient energy to a necessary and sufficient surface area along with supplying sufficient source gases.

6. Conclusion

This document described the technology for simplifying and increasing the performance of the turbine developed in the ECO engine project.

Concerning aerodynamics, test data on the blade design about control of a shock wave on rotor blades of a high-loaded turbine was acquired. Moreover, the performance of a high-loaded high-pressure turbine was demonstrated through rotating tests, the effect of counter rotation was verified through tests and CFD analyses, and a good prospect of materializing a high-loaded high-pressure single-stage turbine with the counter rotation technology was obtained.

Concerning cooling, it was demonstrated that the multi-slot cooling configuration is an excellent cooling configuration that can be applied to a small-size turbine airfoil to which it is difficult to introduce a complicated cooling system or to a three-dimensional airfoil at reasonable costs equivalent to those of conventional cooling systems. It was also demonstrated that the high-efficiency film hole whose hole shape is improved using the existing machining techniques allows the vortex structure on the airfoil surface to change and mixing with main flow to be inhibited, thus making it possible to substantially increase the cooling performance.

Concerning materials, a good prospect of applying the technologies for reducing costs of ingot production, casting and heat treatment to next-generation single crystal superalloys was obtained. By using these technologies, it is expected that it will be possible to manufacture single crystal turbine blades with excellent characteristics without a significant increase in costs compared with the costs of conventionally used single crystal superalloys (such as CMSX-4).

Concerning production, to form a TBC, laser CVD technology was developed as an alternative to EB-PVD, and it was demonstrated based on the results of coating tests conducted on a turbine blade that a coating can be formed on a member having a complicated three-dimensional curved surface shape by performing laser CVD. In addition, conditions for forming a homogeneous TBC on a large-size member were discussed.

– Acknowledgments –

This study was conducted as part of R&D activities of the "Environmentally Compatible Engine for Small Aircraft" project in the Civil Aircraft Fundamental Technology Program implemented by the Ministry of Economy, Trade and Industry, with the support of the New Energy and Industrial Technology Development Organization (NEDO). We would like to extend our sincere appreciation for the cooperation and guidance we received in conducting this study from NEDO, Japan Aerospace Exploration Agency (JAXA), National Institute for Materials Science (NIMS), and Tokyo University of Agriculture and Technology.

REFERENCES

(1) Fujimoto, et al. : Study on Advanced Turbine Cooling Technologies for Development of Next Generation Small Class Airplane Engines, The 47th Conference on Aerospace Propulsion (2007)
(2) Y. Okita and M. Nishiura : Film Effectiveness Performance of an Arrowhead-Shaped Film-Cooling Hole Geometry Journal of Turbomachinery Vol.129 No.2 (2005) pp. 331-339
(3) M. Hamabe, R. Yamawaki, H. Hamazaki and H. Tanimitsu : Numerical Investigation of the Effects of a Counter-Rotating LP Turbine on an Interaction between a HP and the LP Turbine ACGT2005-070
(4) H. Tanimitsu, H. Hamazaki, K. Mitsuhashi and N. Asaumi : Performance Improvement of HP and LP Turbine in ECO Engine ISABE-2007-1220 (2007)
(5) Roger C. Reed : The SUPERALLOYS Fundamentals and Applications CAMBRIDGE UNIVERSITY PRESS pp. 124-125
(6) Y. Aoki, M. Arai, K. Chikugo, Y. Koizumi and H. Harada : Mechanical Properties and Castability of a 4th Generation Ni-base Single Crystal Superalloy TMS-138 IGTC2003 Tokyo TS-118 (2003)